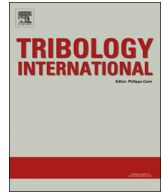




ELSEVIER

Contents lists available at ScienceDirect

Tribology International

journal homepage: www.elsevier.com/locate/triboint

A damage mechanics approach to fretting fatigue life prediction with consideration of elastic–plastic damage model and wear

Fei Shen, Weiping Hu*, Qingchun Meng

Institute of Solid Mechanics, School of Aeronautics Science and Engineering, Beihang University, Beijing 100191, China

ARTICLE INFO

Article history:

Received 12 June 2014

Received in revised form

27 August 2014

Accepted 21 October 2014

Available online 30 October 2014

Keywords:

Fretting fatigue

Continuum damage mechanics

Elastic–plastic

Wear

ABSTRACT

In this investigation an approach to fretting fatigue life prediction is developed with consideration of damage-coupled elastic–plastic constitutive model and wear. Nonlinear kinematic hardening is employed in the analysis of elastic–plastic damage, and the total damage is divided into two parts, elastic damage and plastic damage, which are related to the cyclic stress and accumulated plastic strain, respectively. Wear is modeled by the energy wear law to simulate the evolution of contact geometry. A two dimensional plane strain finite element implementation is presented for fretting, including the case of partial slip and gross sliding. The progressive fatigue damage and wear is simulated and the results are compared with experimental data from the literature.

© 2014 Elsevier Ltd. All rights reserved.

1. Introduction

Fretting is a contact damage process arising from surface micro-slip associated with small scale oscillatory motion of clamped structural members. The contact and relative slip between the components affect the nucleation of fatigue cracks significantly when compared to fatigue situations without fretting. Many components in real service are subjected to fretting, such as bolted and riveted connections, blade–disk attachment in gas and steam turbines [1], hip joint implants [2] and so on. Due to the complexity and the lack of understanding, around 50 variables have been identified as relevant to fretting [3], the effects of which on the fretting fatigue were analyzed in numerous studies. Jin and Mall investigated the influence of contact configuration [4] and slip amplitude [5,6] on fretting fatigue. The effect of contact pressure was studied in the works of Nakazawa et al. [7] and Ramakrishna et al. [8]. It is generally accepted that coefficient of friction, contact pressure and slip amplitude are the primary factor in fretting fatigue.

One approach adopted to predict fretting fatigue life is the critical plane approach, which is based on the multiaxial fatigue model. The method searches for the maximum fatigue parameter, such as Smith–Watson–Topper (SWT), over a number of planes and predicts fatigue life based on the maximum value. Szolwinski and Farris [9] extended a multiaxial fatigue theory that combines strain versus fatigue life ideas with a maximum normal stress to

predict both the location of fatigue cracks and fretting fatigue life. Lykins and Mall [10] evaluated many parameters for predicting fretting fatigue crack initiation, such as strain based fatigue parameters, critical plane based fatigue parameters and Ruiz parameters. However, the critical plane approach employs fatigue parameter to predict fretting fatigue life, which reveals little characteristic of fatigue damage.

The damage mechanics approach also has been introduced to fretting fatigue problem and predicts the evolution of internal damage before macro-cracks become visible. The approach deals with the mechanical behavior of a deteriorated medium on macroscopic scale and evaluates progressive damage accumulated in material until damage reaches a critical value. Damage evolution law derived from thermodynamic is combined with damage-coupled constitution model of material to simulate the evolution of material damage. Zhang et al. [11] developed a coupled damage mechanics approach in conjunction with finite element analysis to predict fretting fatigue life and the results were compared with that predicted by the critical plane method. Hojjati-Talemi et al. [12] used an uncoupled damage evolution law to predict fretting fatigue crack initiation lifetime. Sadeghi et al. [13] proposed a damage mechanics approach, in which the material microstructure was modeled using Voronoi tessellation, to investigate the fretting fatigue, and the variability of fatigue life due to the randomness in material microstructure was also studied. The crack nucleation behavior of rough surfaces in line contact was investigated via damage mechanics method by Aghdam et al. [14]. The stress on the contact surface and sub-surface are used to estimate fretting fatigue life for the unworn and elastic loading case. However, the effect of wear caused by relative slip between the contacting components is not considered in the damage

* Correspondence to: Room D604, New Main Building, 37th Xueyuan Road, Beihang University, Beijing 100191, China. Tel.: +86 1082338489.

E-mail address: huweiping@buaa.edu.cn (W. Hu).

mechanics approaches mentioned above. Besides, plastic deformation can occur in the contact zone due to the evolution of contact geometry induced by wear [3]. The effect of cyclic plasticity needs to be considered when plastic deformation occurs.

The effect of wear on the contact surface and sub-surface contact variables, such as contact pressure, slip, stresses and critical plane parameters is widely studied. McColl et al. [15] developed a finite element simulation for fretting wear based on a modified Archard wear model. Madge et al. [16,17] combined modified Archard wear model with critical plane method to successfully evaluate the effect of fretting wear on fretting fatigue life. A combined finite–discrete element method was employed to model the fretting wear of coated and uncoated surfaces by Leonard et al. [18]. Zhang et al. [19] predicted fretting performance of two different contact geometries with the adoption of energy wear model proposed by Fouvry et al. [20]. The energy wear model has been shown to be superior to the Archard-based approach in that a single wear coefficient can be used across a range of fretting load–stroke combinations, specifically including both partial slip and gross sliding regimes [19]. Recently, Sadeghi et al. [21] proposed a damage mechanics approach to simulate wear at the level of material microstructure and the results of the simulation are compared with the Archard wear law. The damage mechanics approach was employed to simulate crack nucleation, propagation and element deletion, leading to the progression of the wear scar. When considering the effect of wear, the predicted fretting fatigue life is more reasonable, especially for the case of gross sliding. However, the fretting fatigue life was predicted by combining the critical plane fatigue model and wear model in the literatures [16,17,19] and the Miner–Palmgren rule was adopted to accumulate the fatigue damage, which is a linear accumulation law and ignores the effect of loading sequence. The damage accumulation is carried out after the numerical simulation of wear.

The present work is concerned with fretting fatigue crack initiation behavior. Fretting fatigue damage and wear is considered simultaneously in the damage mechanics approach. The effects of the fatigue damage and wear are coupled with each other. Damage evolution law and energy wear law are used to model the fatigue damage and wear based on the calculated stress and strain by damage-coupled elastic–plastic constitutive model, respectively. A numerical implementation of these models is developed with the commercially available ABAQUS finite element software to simulate the evolution of fatigue damage and wear scar. The predicted results are compared with experimental data from the literature.

2. Theoretic background

2.1. Damage-coupled elastic–plastic constitutive model

Lemaitre and Chaboche [22] have presented some fundamental concepts in damage mechanics. A number of continuum models and micromechanical models for material damage were presented in the literature [23]. Damage in its mechanics sense in solid materials is the creation and growth of micro-voids or micro-cracks which are discontinuities in a medium considered as continuous at a larger scale. A damage variable is introduced to estimate the progressive deterioration of material due to fatigue loading. In this study isotropic damage is assumed and the damage variable D is a scalar.

In the framework of small deformation, total strain ϵ_{ij} can be divided as

$$\epsilon_{ij} = \epsilon_{ij}^e + \epsilon_{ij}^p \quad (1)$$

where ϵ_{ij}^e and ϵ_{ij}^p are elastic strain and plastic strain, respectively. In the damage-couple constitutive model, damage is coupled with

elasticity and plasticity by using the effect stress instead of the stress in the elasticity law and Mises yield criterion based on the strain equivalent principle [24]. The elastic strain takes the form

$$\epsilon_{ij}^e = \frac{1+\nu}{E} \left(\frac{\sigma_{ij}}{1-D} \right) - \frac{\nu}{E} \left(\frac{\sigma_{kk} \delta_{ij}}{1-D} \right) \quad (2)$$

where E , ν and σ_{ij} are elastic modulus, Poisson's ratio and Cauchy stress, respectively. The evolution of plastic strain is defined as

$$\dot{\epsilon}_{ij}^p = \dot{\lambda} \frac{\partial F}{\partial \sigma_{ij}} \quad (3)$$

where $\dot{\lambda}$ is the plastic multiplier and F is the Mises yield function with damage defined as

$$F = \sqrt{\frac{3}{2} \left(\frac{s_{ij}}{1-D} - \alpha_{ij} \right) \left(\frac{s_{ij}}{1-D} - \alpha_{ij} \right)} - Q \quad (4)$$

where s_{ij} is the deviatoric part of stress and α_{ij} is the deviatoric part of back stress. Q is the radius of yield surface and its evolution is defined as

$$\dot{Q} = \dot{\lambda} b (Q_\infty - Q) \quad (5)$$

where parameters b and Q_∞ are material constants determined experimentally. The rate equation of plastic strain is deduced as

$$\dot{\epsilon}_{ij}^p = \frac{3}{2} \frac{\dot{\lambda}}{1-D} \frac{(s_{ij}/(1-D)) - \alpha_{ij}}{((s_{ij}/(1-D)) - \alpha_{ij})_{eq}} \quad (6)$$

Then the plastic multiplier $\dot{\lambda}$ is determined by applying the consistency condition

$$\dot{p} = \sqrt{\frac{2}{3} \dot{\epsilon}_{ij}^p \dot{\epsilon}_{ij}^p} = \frac{\dot{\lambda}}{1-D} \quad (7)$$

where \dot{p} is the accumulated plastic strain rate.

For accurate estimation of the yield surface movement, the deviatoric part of back stress is divided into finite components. Each component is modeled based on the Armstrong and Frederick [25] nonlinear kinematic hardening (NLKH) model, which has the advantage of reducing the computational time due to the simplicity. It is to be noted that this model may overestimate the accumulation of plastic strain [26–28]. The evolution law of nonlinear kinematic hardening rule is

$$\alpha_{ij} = \sum_{k=1}^M \alpha_{ij}^{(k)} \quad (8)$$

$$\dot{\alpha}_{ij}^{(k)} = (1-D) \left(\frac{2}{3} C_k \dot{\epsilon}_{ij}^p - \gamma_k \alpha_{ij}^{(k)} \dot{p} \right) \quad (9)$$

where C_k and γ_k are material constants also determined experimentally.

2.2. Damage evolution models

The contact conditions, including contact geometry and material properties, vary from cycle to cycle, leading to the occurrence of plastic strain. The elastic damage law [11,12] cannot simulate the evolution of damage for material point with plastic strain well. A plastic damage law is needed to model the plastic damage induced by the plastic strain. In general, the evolution of damage for a material point can be calculated by either the elastic damage evolution law or the plastic damage evolution law depending on the current stress status in a cycle [29]. However, the plastic strain in the fretting fatigue is small and only the plastic damage increment is not adequate to represent the evolution of damage when plastic deformation occurs. Therefore, the total damage is divided into two parts, elastic damage and plastic damage, in the present study. The elastic damage is merely dependent on the state of cyclic stress and the plastic damage is governed by the

accumulated plastic strain over each fatigue cycle. The strategy for calculating the total damage is introduced in Section 4.3.

The elastic damage evolution model [22,30,31] is written as follows:

$$\frac{dD^e}{dN} = \left[1 - (1-D)^{\beta+1} \right]^\eta \left[\frac{A_{II}}{M_0(1-3b_2\sigma_{H,mean})(1-D)} \right]^\beta \quad (10)$$

where A_{II} is the amplitude of octahedral shear stress, expressed by

$$A_{II} = \frac{1}{2} \left[\frac{3}{2} (S_{ij,max} - S_{ij,min})(S_{ij,max} - S_{ij,min}) \right]^{1/2} \quad (11)$$

where $S_{ij,max}$ and $S_{ij,min}$ are the maximum and minimum values of the deviatoric stress during one loading cycle respectively. $\sigma_{H,mean}$ is the mean value of hydrostatic stress:

$$\sigma_{H,mean} = \frac{1}{6} (\sigma_{kk,max} + \sigma_{kk,min}) \quad (12)$$

Parameter η is defined with the Sines fatigue limit criterion [32] as

$$\eta = 1 - a \left\langle \frac{A_{II} - A_{II}^*}{\sigma_u - \sigma_{eq,max}} \right\rangle \quad (13)$$

$$A_{II}^* = \sigma_{I0} (1 - 3b_1\sigma_{H,mean}) \quad (14)$$

where $\sigma_{eq,max}$ is the maximum equivalent stress over a loading cycle. σ_{I0} is the fatigue limit at the fully reversed loading condition and σ_u is the ultimate tensile stress. Five parameters, a , M_0 , β , b_1 , b_2 , are determined by using plain fatigue tests of standard specimens.

The plastic damage evolution model [24,33,34] dependent on accumulated plastic strain is given by

$$\frac{dD^p}{dN} = \left[\frac{(\sigma_{max}^*)^2}{2ES(1-D)^2} \right]^m \dot{p} \quad (15)$$

where σ_{max}^* is the maximum value of damage equivalent stress [24] over a loading cycle. Damage equivalent stress is defined as

$$\sigma^* = \sigma_{eq} R_v^{1/2} \quad (16)$$

$$R_v = \frac{2}{3}(1+\nu) + 3(1-2\nu) \left(\frac{\sigma_H}{\sigma_{eq}} \right)^2 \quad (17)$$

Parameters S and m are determined by reference to the experimental data of plastic strain versus number of cycles curve. The detailed procedure to identify the parameters is presented in Section 3.

2.3. Wear model

The energy wear model considers the interfacial shear work as the significant wear parameter controlling wear volume calculation, which is represented by

$$V = \phi \Sigma W \quad (18)$$

where ϕ is wear coefficient and ΣW is the accumulated dissipated energy. For 2D fretting model, at time t and position x along the contact surface, the local wear depth can be expressed as follows [19]:

$$h(x, t) = \phi \int_{t=0}^t q(x, t) ds(x, t) \quad (19)$$

where $q(x, t)$ is the local shear traction and $ds(x, t)$ is the local incremental relative slip.

Fridrici et al. [35] have studied the fretting wear of Ti-6Al-4V by using the energy wear model with wear coefficient value of $2.9 \times 10^{-8} \text{ MPa}^{-1}$. Meanwhile, wear coefficient with a value of $7.121 \times 10^{-7} \text{ MPa}^{-1}$ was adopted to investigate the wear characterization of Ti-6Al-4V under fretting-reciprocating sliding

conditions by Magaziner [36]. The difference of wear coefficient value in two papers can be attributed to several factors discussed in the literature [36]. The relative slip in the study of Magaziner was about one order of magnitude higher than that used in the present study. In addition, the hardness used by Fridrici was higher than that of the present study due to the shot peening. With the consideration of material mechanical constants and fretting loading conditions in this study, a value of wear coefficient is chosen to fall in between the two values mentioned above, which is $2 \times 10^{-7} \text{ MPa}^{-1}$. The appropriateness of this value will be validated by the wear analysis and fatigue life prediction.

3. Material and parameters identification

In this section, the procedures to identify the material parameters of aforementioned models for Ti-6Al-4V are presented.

3.1. Elastic-plastic constitutive model parameters

The experimental data of uniaxial monotonic tension stress-strain curve [37] is used for the determination of back stress constants. The isotropic hardening is neglected in this study, which means the size of yield surface remains unchanged. In the finite element implementation, the parameters b and Q_∞ are set to be 1.0 and 0, respectively. The isotropic hardening becomes

$$Q = \sigma_y \quad (20)$$

where σ_y is the initial yield stress.

For the case of uniaxial loading, each component of back stress is approximated using an exponential saturation equation described as follows:

$$\alpha^{(k)} = \frac{C_k}{\gamma_k} (1 - e^{-\gamma_k \epsilon_p}) \quad (21)$$

Then the stress-strain curve is expressed as

$$\sigma = \sigma_y + \sum_{k=1}^M \frac{C_k}{\gamma_k} (1 - e^{-\gamma_k \epsilon_p}) \quad (22)$$

where σ and ϵ_p are the stress and plastic strain respectively. The least square method is employed to determine the parameters according to the experimental data and the result of data fitting is shown in Fig. 1. Table 1 lists the mechanical properties and material parameters for Ti-6Al-4V.

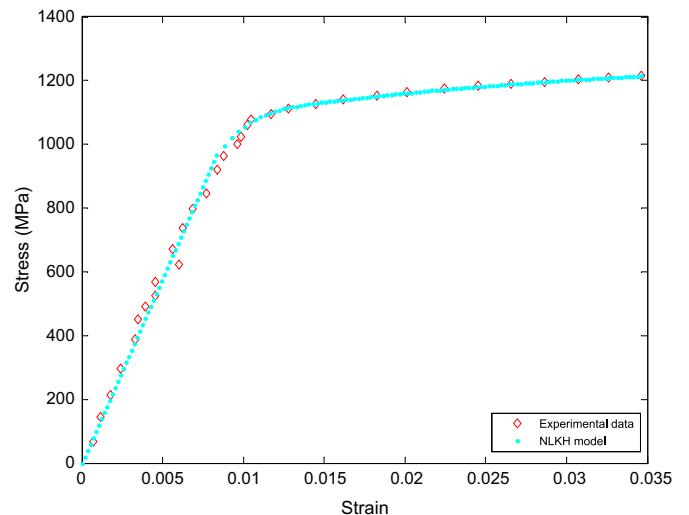


Fig. 1. Uniaxial monotonic tension stress-strain curve for Ti-6Al-4V.

Table 1
Mechanical properties and material parameters for Ti-6Al-4V.

E (MPa)	ν	σ_y (MPa)	C_1 (MPa)	C_2 (MPa)	γ_1	γ_2
116,000	0.34	965	136,500	8100	1050	45

3.2. Parameters identification for damage evolution models

Several parameters for two different damage evolution models, elastic damage model and plastic damage model, need to be determined. The experimental fatigue tests of standard specimens are employed to obtain the parameters in the damage evolution models.

3.2.1. Parameters identification for elastic damage evolution model

For uniaxial fatigue, the number of cycles to failure for a given stress condition is obtained by integrating Eq. (10) from $D = 0$ to $D = 1$, leading to

$$N_F = \frac{1}{1 + \beta} \frac{1}{aM_0^{-\beta}} \frac{\langle \sigma_u - \sigma_{max} \rangle}{\langle \sigma_a - \sigma_{10}(1 - b_1 \bar{\sigma}) \rangle} \left[\frac{\sigma_a}{1 - b_2 \bar{\sigma}} \right]^{-\beta} \quad (23)$$

where σ_{max} , σ_a and $\bar{\sigma}$ are the maximum stress, stress amplitude and mean stress during a loading cycle, respectively.

The ultimate tensile stress σ_u is obtained from monotonic tensile stress-strain curve. Parameters σ_{10} and b_1 are obtained from the fatigue limit data at different mean stress. Parameters β and $aM_0^{-\beta}$ can be obtained from stress-controlled fatigue test at fully reversed loading condition. Parameter b_2 can be obtained from fatigue tests at different mean stress. Parameter a is obtained according to the method introduced by Zhang [11]. The fatigue tests data of material Ti-6Al-4V is from Ref. [37] and the parameters for the elastic damage evolution model are listed in Table 2. Fig. 2 shows the experimental fatigue data and predicted curves for standard specimens.

3.2.2. Parameters identification for plastic damage evolution model

The parameters in the plastic damage evolution model are obtained by equating the integral of the damage evolution model and plastic strain versus number of cycles curve. Using Coffin-Manson law, the equation of plastic strain versus number of cycles curve can be written as

$$\frac{\Delta \epsilon_p}{2} = \epsilon_f (2N_f)^c \quad (24)$$

where ϵ_f is the fatigue ductility coefficient and c is the fatigue ductility exponent. The integrated damage evolution equation, Eq. (15), for uniaxial case is

$$N_F = \frac{1}{2(2m+1)\Delta \epsilon_p} \left(\frac{2ES}{(\sigma_{max})^2} \right)^m \quad (25)$$

By using the cyclic stress-strain curve

$$\sigma_{max} = K' \left(\frac{\Delta \epsilon_p}{2} \right)^{n'} \quad (26)$$

where K' and n' are parameters obtained from experiments. Then Eq. (25) can be written as

$$N_F = \frac{1}{2(2m+1)} \left(\frac{2^{1+2n'} ES}{(K')^2} \right)^m (\Delta \epsilon_p)^{-(1+2mn')} \quad (27)$$

By using the data of plastic strain versus number of cycles curve [38], the values of ϵ_f , c , K' and n' are obtained. After that, the parameters in the plastic damage evolution model are determined and listed in Table 3.

Table 2
Parameters for elastic damage evolution model for Ti-6Al-4V.

σ_u (MPa)	σ_{10} (MPa)	β	$aM_0^{-\beta}$	b_1	b_2	a
1180	358	2.1	1.79e-11	0.0013	0.00055	0.75

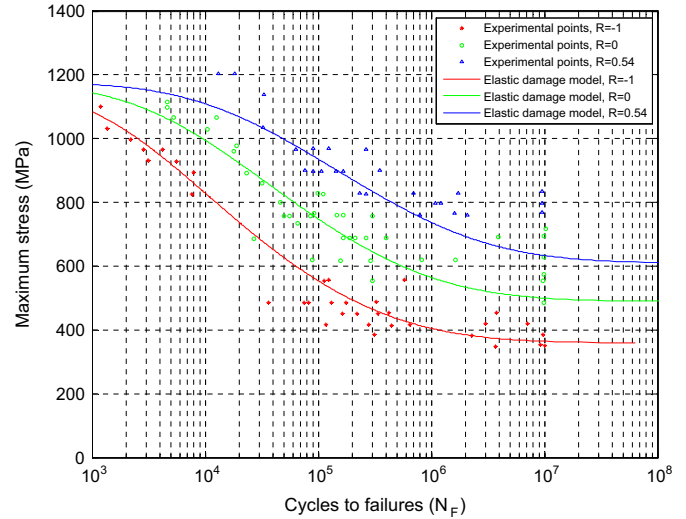


Fig. 2. Experimental fatigue data and predicted curves for standard specimens.

Table 3
Parameters for plastic damage evolution model for Ti-6Al-4V.

S	m
9.9293	4.7846

4. Computational methodology

4.1. Finite element model

The general purpose, non-linear, finite element code ABAQUS is used here. A 4-node (bilinear), plane strain quadrilateral, incompatible modes element (CPE4I) is used in this study. The finite element model is based on the experiment configuration in the literature [5]. The radius of pad is 50.8 mm and the width and thickness of specimen are 6.4 and 3.8 mm, respectively. The contact between the fretting pad and the specimen is defined using the master-slave algorithm for contact between surfaces. Part of the top surface of specimen is defined as the slave surface and part of the circular surface of pad is defined as the master surface. The initial adjustment of contact surface, ADJUST parameter, is used. Coulomb friction is employed based on the Lagrange multiplier contact algorithm to ensure the exact stick condition when the shear stress is less than the critical shear value according to the Coulomb friction law. The constant coefficient of friction COF of $\mu = 0.8$ is considered throughout the analyses [11,17].

The loads are applied in three steps. The normal pressure load P is exerted, in the first two steps and remains unchanged in the third step, by using the Multi-Point Constraint (MPC). In the first step, normal pressure load with a small value is applied on the top surface of pad to establish the contact between the specimen and the pad then the value will be increased to the experimental value, 208 N/mm, in the second step. The axial stress σ_{axial} is applied at the right side of specimen in the third step, which has a maximum

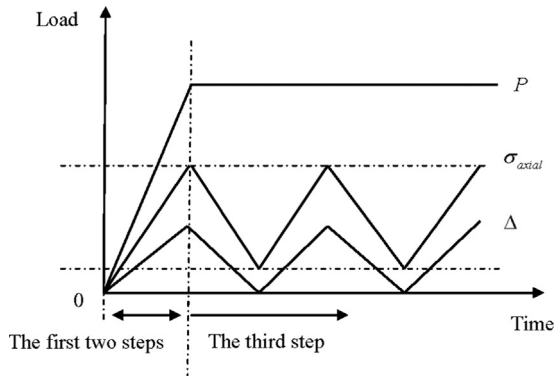


Fig. 3. Schematic of fretting loading history.

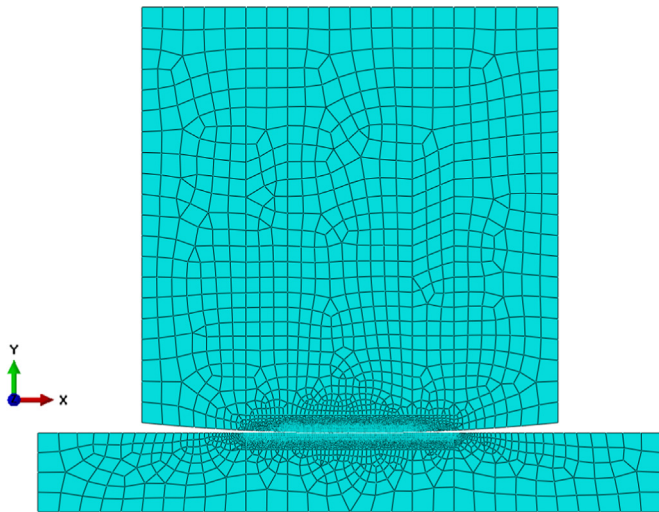


Fig. 4. Finite element model of fretting fatigue.

value of 550 MPa and stress ratio of 0.03. The in-phase stroke Δ is applied to the fretting pad with axial fatigue stress in the third step. Fig. 3 shows the schematic of fretting loading history. The top surface and two sides of the fretting pad are constrained linearly in order to preclude the occurrence of a tilting moment.

Fig. 4 shows the finite element model of fretting fatigue configuration. The element length and width on the contact surface are both $10\ \mu\text{m}$. A mesh convergence study is conducted to validate the appropriateness of current mesh size at contact region between the pad and the specimen. The comparisons between theoretical solutions and finite element results are presented below.

It has been pointed out by Jin and Mall [5] that the finite element predicted slip magnitudes associated with the transition from partial slip to gross sliding do not agree with these Ti-6Al-4V tests. The local relative slip amplitude δ_{local} computed in finite element simulation is significantly smaller than the experimentally observed relative slip amplitude δ_{global} , since the global relative slip incorporates the effects of rig compliance and the surface conditions. The relationship between the local slip amplitude and global slip amplitude is expressed [17,39]:

$$\delta_{local} = \delta_{global} \frac{C_{COF}}{C_{rig}} \quad (28)$$

where C_{COF} , C_{rig} are constants which account for the effect on compliance of COF and rig compliance, respectively. In this study, the resulting value of C_{rig}/C_{COF} is 16 based on the data in the literature [39].

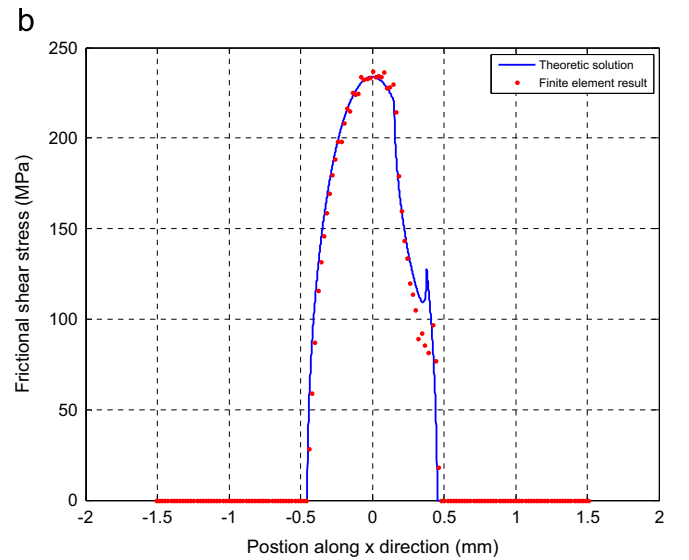
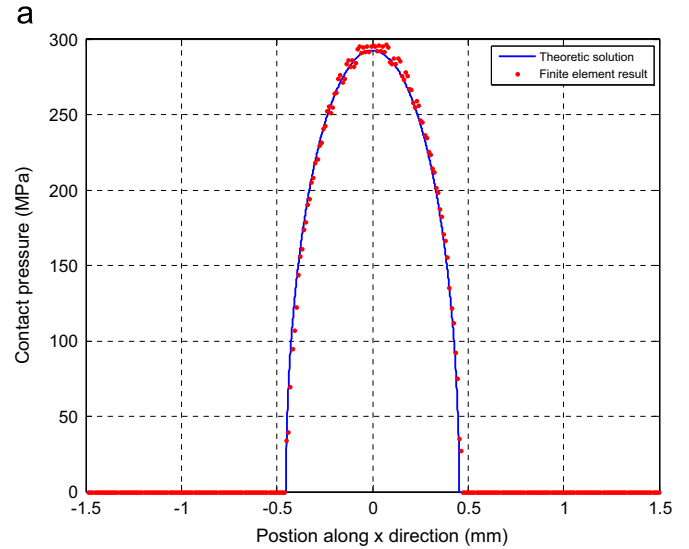


Fig. 5. Comparisons of theoretic solutions and finite element results of (a) contact pressure and (b) shear traction ($Q=150\ \text{N/mm}$).

4.2. Validation of finite element model

For the sake of simplicity, the loading condition for the validation is specified to meet the equation [1]:

$$\frac{\sigma_{axial}}{\mu p_0} \leq 4 \left(1 - \sqrt{1 - \frac{Q}{\mu P}} \right) \quad (29)$$

which makes sure that there are closed forms for the equations in the theoretic solution [1,40]. In the above equation, p_0 is the peak contact pressure and Q is frictional tangential force. Fig. 5(a) and (b) shows the comparisons of finite element results of contact pressure and shear traction along the contact surface with the theoretical solutions. The small differences in both comparisons may be attributed to two main reasons: (1) the elastic half-space assumption of the theoretic solution is not quite satisfied since the contact semi-width of $0.453\ \text{mm}$ is of comparable magnitude to the specimen thickness of $1.9\ \text{mm}$ and (2) the finite element calculation employs a large deformation assumption whereas the theoretic solution is based on a small deformation assumption.

4.3. Numerical implementation

The approach involves the simulation of the damage-coupled elastic–plastic constitutive model, damage evolution models and wear model. The constitutive model and damage evolution models are implemented through the user subroutine UMAT in ABAQUS, which is called at all material integration points at the beginning of each time increment. The user subroutine updates the stress and solution-dependent state variables to their values at the end of time increment, which is followed by the updating of corresponding Jacobian matrix. The main body of the procedure is the implementation of implicit stress integration algorithm and evolution of consistent elastic–plastic tangent modulus [41–44]. Since it is computationally expensive to simulate each loading cycle, the jump-in-cycles procedure [24] is adopted in the numerical implementation, which assumes that the stress, accumulated plastic strain and damage remain unchanged for a finite period of ΔN cycles constituting a block. Then the damage evolution can be interpreted as piecewise linear with respect to the number of cycles. It is necessary to note that the value of ΔN is determined to obtain a convergent fretting fatigue life.

The wear model is also implemented in ABAQUS through the user subroutine UMESHMOTION. The adaptive meshing user subroutine is called after the equilibrium iteration of each time increment to simulate the material removal according to the wear model. The jump-in-cycles procedure is also employed. A simplified flowchart of the total algorithm used in this study is shown in Fig. 6 and the detailed steps of the numerical implementation are listed as follows:

- (1). The initial damage for each element is assumed to be zero.
- (2). The damage-coupled elastic–plastic constitutive rate equations, Eqs. (1)–(9), are solved to obtain the stress, elastic and plastic strain. The stress and accumulated plastic strain histories are calculated for the current block.
- (3). During each block, three steps to implement the wear model are listed as follows:

- (a) For a contact node, the increment of local wear depth at the k th time increment for a block is written as

$$\Delta h = \phi \Delta N q_k \Delta s_k \tag{30}$$

where q_k and Δs_k are shear traction and incremental slip at the k th time increment, respectively. The increment of local wear depth, Δh , is implemented by moving the surface nodes in the local normal direction at the end of each time increment. This geometry update is implemented as a purely Eulerian analysis.

- (b) The material variables are re-mapped to the new position, by advection from old location to the new location, by solving the advection equations using a second order numerical method called the Lax–Wendroff method [45].
- (c) Repeat (a) and (b) until the number of time increment k reaches the maximum number of time increment within one fretting cycle, M_{max} . In this study, $M_{max} = 100$.

- (4). After each block, three steps to compute damage and update material properties are listed as follows:

- (a) According to the stress and accumulated plastic strain histories, the damage evolution rate is calculated using two damage evolution models, Eqs. (10) and (15). The total damage evolution rate for each element is obtained by adding two damage evolution rates.

$$\left(\frac{dD}{dN}\right)_j^i = \left(\frac{dD^e}{dN}\right)_j^i + \left(\frac{dD^p}{dN}\right)_j^i \tag{31}$$

where i represents the current block and j is the number of element. If no plastic deformation occurs, the plastic damage evolution rate vanishes and the elastic damage

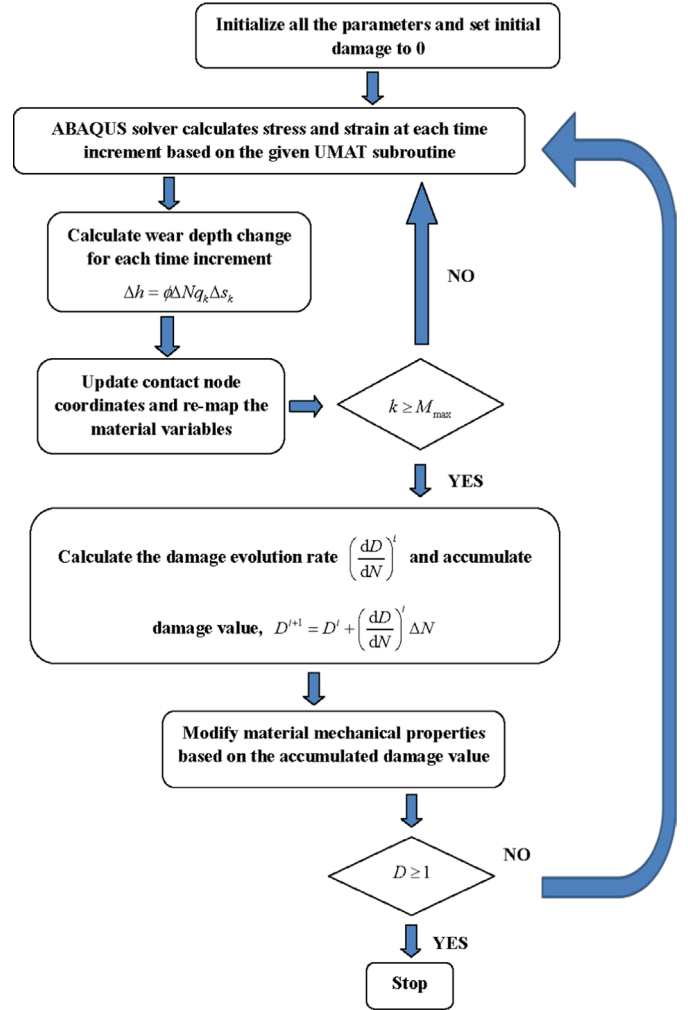


Fig. 6. Simplified flowchart of the entire algorithm.

evolution rate is the total damage evolution rate, which is the same as the method used in the literatures [11,12].

- (b) The damage values and the number of cycles for all elements are updated at the end of current block.

$$D_j^{i+1} = D_j^i + \left(\frac{dD}{dN}\right)_j^i \Delta N \tag{32}$$

$$N^{i+1} = N^i + \Delta N \tag{33}$$

- (c) Material properties are modified based on the calculated damage value for the next block. The properties involve elastic modulus, C_k and γ_k .

$$\text{Property}_j^{i+1} = \text{Property}(1 - D_j^{i+1}) \tag{34}$$

- (5). The algorithm repeats steps (2)–(4) for each block of cycles until the accumulated damage of any integration point reaches the critical value D_c . The number of cycles at this stage is the fretting fatigue crack initiation life. In this study, the critical value is set to 1.

5. Results and discussion

The strokes applied in this study and corresponding local slip amplitudes are listed in Table 4, five of which are the cases of

Table 4
Applied strokes and local slip amplitudes.

Δ (μm)	32.1	35	35.56	40	42	43	44
δ_{local} (μm)	1.357	2.047	2.208	3.633	4.408	5.262	6.249
Slip regime	p.s.	p.s.	p.s.	p.s.	p.s.	g.s.	g.s.

Note: p.s. – partial slip and g.s. – gross sliding.

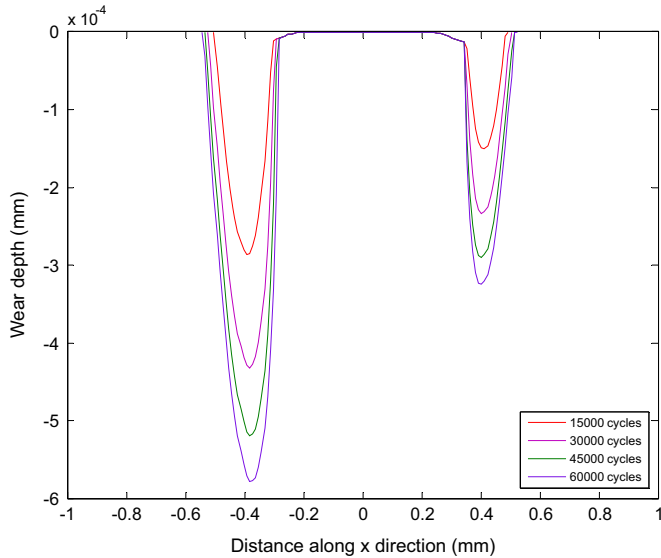


Fig. 7. Evolution of wear scar distribution for $\Delta = 32.1 \mu\text{m}$.

partial slip and two of which are the cases of gross sliding. According to the fretting fatigue tests data in the literature [5], the partial slip-gross sliding threshold is around $4.7 \mu\text{m}$, which agrees well with the computed threshold in Table 4.

5.1. Wear simulation results

The evolution of wear scar is accompanied by the evolution of fatigue damage in the numerical algorithm. The contact geometry is updated by moving the coordinates of contact node. Once the fretting fatigue crack occurs, the simulation of wear ends. No element deletion is simulated in this study.

5.1.1. Partial slip case

The predicted wear scar corresponding to the partial slip case for $\Delta = 32.1 \mu\text{m}$ is presented in Fig. 7. No wear is predicted in the central stick zone and the wear depths of two slip zones are predicted to increase with cycling. The wear scar at the left slip zone is deeper than that at the right slip zone. Compared to the symmetrical wear scar in the literature [19], the reason of the unsymmetrical wear scar in this study can be attributed to the existence of axial fatigue stress and unsymmetrical stroke as shown in Fig. 4. The width of total contact zone increases slightly with cycling, and the width of central stick zone remains unchanged. These results agree well with the results from the literature [17].

Fig. 8(a) and (b) depicts the evolution of the distribution of contact pressure and shear traction along the contact surface for $\Delta = 32.1 \mu\text{m}$. The contact pressure in the central stick zone increases slightly with increasing cycles, while the contact pressure peaks at the two stick-slip interfaces $x = -0.274, 0.347 \text{ mm}$ increase significantly with cycling. Partial slip causes a transfer of pressure to the stick region, while the slip regions are worn away and hence pressure is relieved. It approaches a punch on flat contact. The

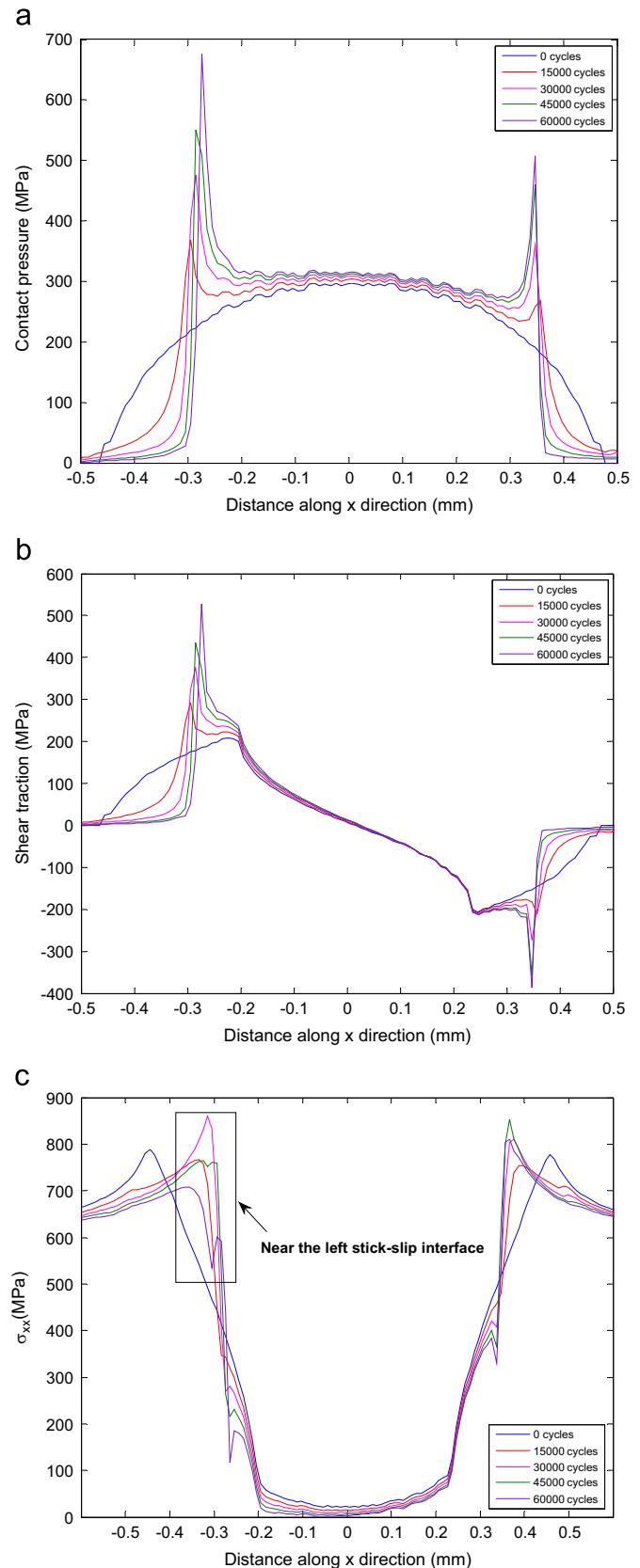


Fig. 8. Evolution of the distribution of (a) contact pressure, (b) shear traction and (c) σ_{xx} for $\Delta = 32.1 \mu\text{m}$.

maximum shear traction is predicted at the left stick-slip interface and increases with cycling. The shear traction in the stick region remains nearly unchanged. Fig. 8(c) shows the distribution of σ_{xx}

along the contact surface after different numbers of cycles. Initially two peaks of stress are at the contact edge $x = \pm 0.45$ mm and gradually move towards the stick–slip interfaces. This trend is the same as that predicted by Mohd Tobi et al. [3].

Fig. 9 shows the evolution of equivalent plastic strain distribution along the contact surface for $\Delta = 32.1 \mu\text{m}$. The plastic strain is predicted to occur firstly at the left stick–slip interface $x = -0.274$ mm after 24,000 cycles and increases significantly. At the right stick–slip interface $x = 0.347$ mm, plastic deformation takes place after 42,000 cycles.

The accumulated damage value along the contact surface evolves with increasing cycles, as shown in Fig. 10. The damage distribution is localized at two stick–slip interfaces. Two peaks are near stick–slip interfaces and maximum damage is at the location of $x = -0.31$ mm. Before the occurrence of plastic deformation, the maximum damage value is about 0.09, which is obtained by accumulating the elastic damage. The plastic damage is accumulated to the total damage with the existence of plastic strain. However, the plastic damage is much less than the elastic damage for $\Delta = 32.1 \mu\text{m}$. The plastic damage increment dD^p/dN at the location of crack initiation is about 1.42×10^{-6} after 70,000 cycles

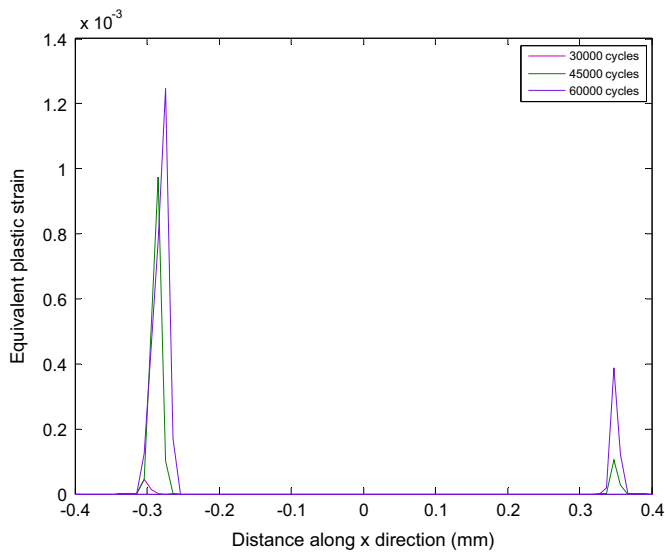


Fig. 9. Evolution of equivalent plastic strain distribution for $\Delta = 32.1 \mu\text{m}$.

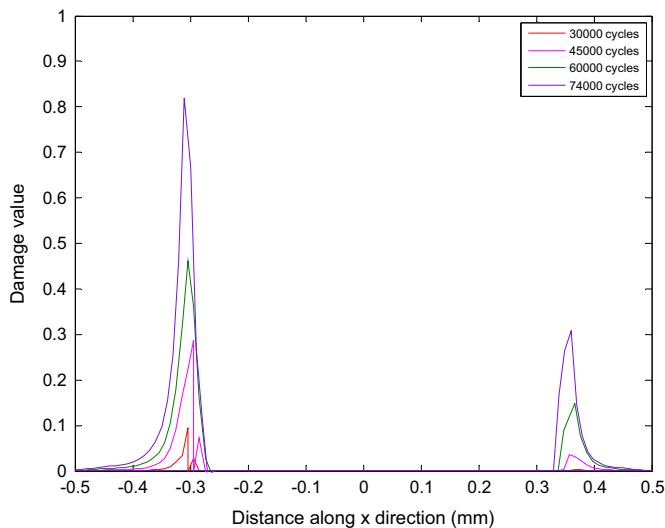


Fig. 10. Evolution of damage distribution for $\Delta = 32.1 \mu\text{m}$.

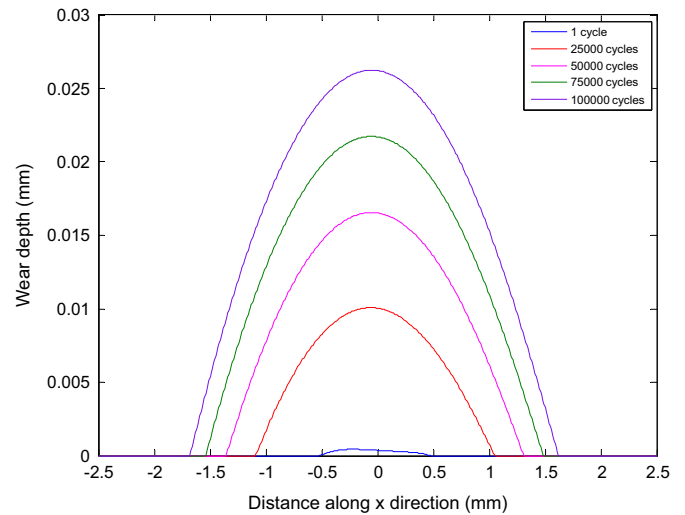


Fig. 11. Evolution of wear scar distribution for $\Delta = 43 \mu\text{m}$.

while the elastic damage increment dD^e/dN is 2.65×10^{-5} , about 20 times the plastic damage increment.

5.1.2. Gross sliding case

Fig. 11 shows the predicted wear scar evolution along the contact surface for $\Delta = 43 \mu\text{m}$. The shape of wear scar after a number of cycles is U-shape as similar as the predicted wear profile in the literatures [3,19]. However the wear scar after the first cycle is unsymmetrical due to the unsymmetrical distribution of relative slip along the contact surface. The distribution of shear traction is symmetrical for the first cycle. However, the value of relative slip at the left contact edge is $5.262 \mu\text{m}$ while at right contact edge is $0.886 \mu\text{m}$. The minimum relative slip is near the right contact edge, which results in that the maximum wear depth is near the left contact edge, as shown in Fig. 11. Another obvious trend depicted in Fig. 11 is the widening of contact zone, which affects the contact stresses and other mechanical variables significantly. The total contact zone widens with increasing cycles, from 0.9 mm to 3.3 mm. However, the predicted wear scar is different from the experimental wear profile which is W-shape [36]. The energy wear model needs to be improved to obtain the W-shape scar, which is still an unsolved problem.

The wear scar has significant effect on contact pressure distribution for $\Delta = 43 \mu\text{m}$ as shown in Fig. 12(a). The contact pressure starts with a Hertzian shape, corresponding to the unworn case. The mean pressure drops due to the predicted widening of the wear scar. The maximum contact pressure is near or at the right contact edge due to two reasons: (1) the existence of axial fatigue stress on the specimen and the unsymmetrical stroke and (2) the worn–unworn interface at the right contact edge. It is worth pointing out that Fig. 12 is plotted for the time of maximum axial fatigue stress and horizontal slip displacement. Therefore, the distribution of contact pressure moves toward the positive direction of x axis, which is the direction of loading, as the contact zone widens with cycling. The right edge of contact pressure coincides with the distribution of wear scar, which is at $x = 1.66$ mm but the left edge is not identical. The shear traction has the similar distribution as contact pressure because the equation between shear traction and contact pressure, $q = \mu p$, exists for the gross sliding case. Fig. 12(b) shows the distribution of σ_{xx} along the contact surface for different number of cycles. The maximum horizontal displacement of the pad is larger than the displacement due to the specimen strain caused by the axial fatigue stress, which leads to the frictional force with positive direction on the contact surface of the specimen. Material near the left contact edge is stretched and material near the right contact edge is compressed

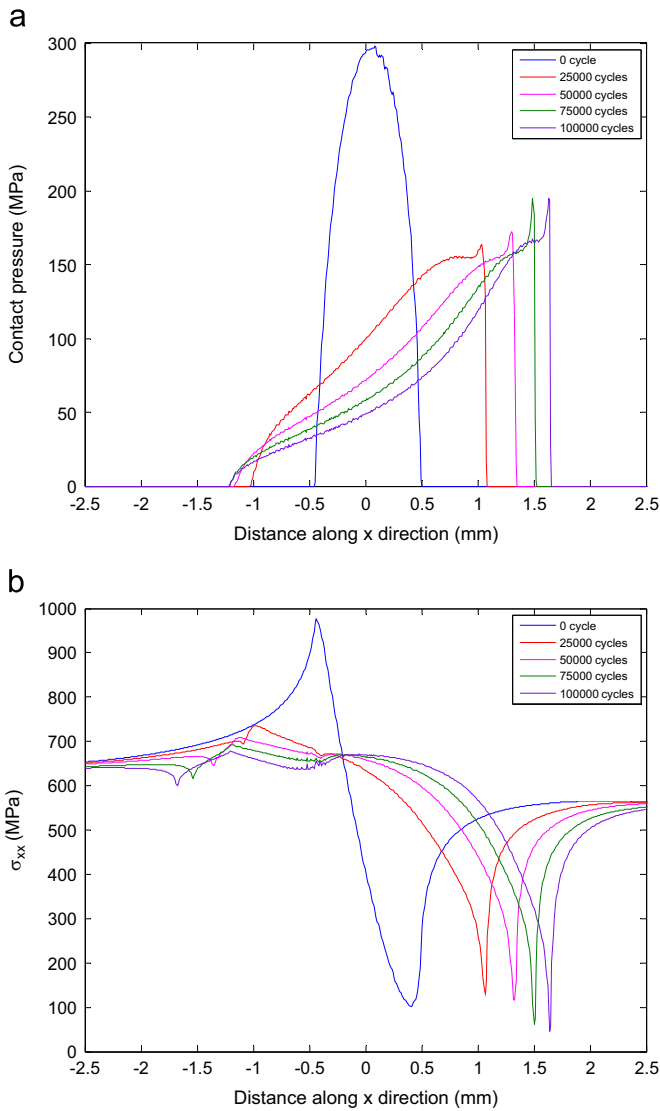


Fig. 12. Evolution of the distribution of (a) contact pressure, (b) σ_{xx} for $\Delta = 43 \mu\text{m}$.

due to the frictional force. For the unworn case, the peak of σ_{xx} is at the left contact edge and the valley is at the right contact edge. The maximum value of σ_{xx} decreases with increasing cycles, the position of which moves from $x = -0.44 \text{ mm}$ to $x = -1.2 \text{ mm}$. The valley moves steadily from the initial right contact edge $x = 0.42 \text{ mm}$ to the wear-induced right contact edge $x = 1.66 \text{ mm}$. The stress σ_{xx} is a key stress component controlling the fatigue damage. A comparison between the distributions of σ_{xx} for the unworn case at different strokes is shown in Fig. 13. As the stroke increases, the peak value increases until reach a steady value. Compared to the contact pressure and shear traction, the stress component σ_{xx} is important due to the larger peak value near the contact edge.

Fig. 14 shows the evolution of damage distribution along the contact surface for $\Delta = 43 \mu\text{m}$. Compared to the partial slip case, the damage distribution is more widespread for the gross sliding case. Due to the widening contact zone, plastic deformation does not exist within the first 100,000 cycles. The damage zone is at the place where the stress component σ_{xx} is high, as depicted in Fig. 12(b). The peak of damage distribution slightly moves left, which is out of initial contact zone.

5.2. Fretting fatigue results

In this study, the damage variable, D , is defined to represent the degradation of material. The contact geometry is changed due to wear

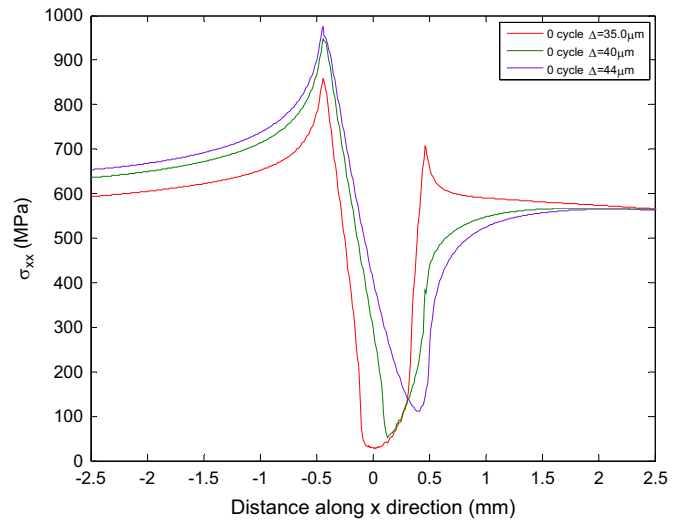


Fig. 13. Distribution of σ_{xx} for the unworn case at different strokes.

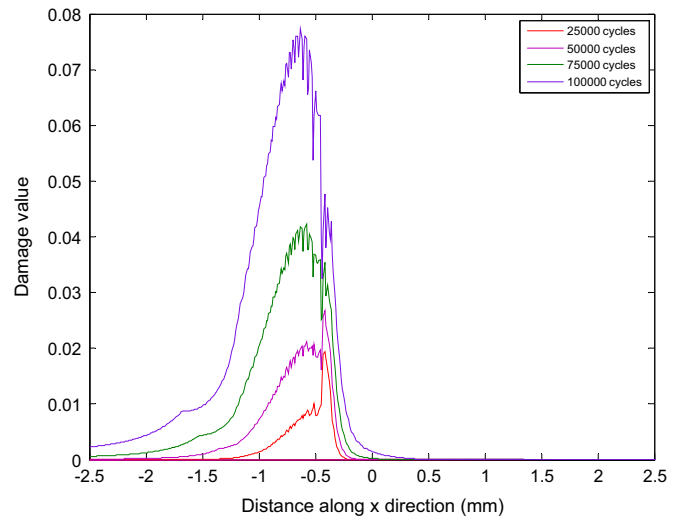


Fig. 14. Evolution of damage distribution for $\Delta = 43 \mu\text{m}$.

and the corresponding stress and strain are calculated based on the damage-coupled constitutive model in each block of cycles. The damage increment is calculated by the damage evolution models and the damage variable is updated after each block of cycles. Once the damage value of any integration point reaches 1, the nucleation of fretting crack occurs and the algorithm ends. The number of loading cycles at this stage is the predicted life of fretting fatigue crack initiation.

Table 5 summarizes the predicted results of crack initiation position and fretting fatigue life, as well as the positions of stick-slip interfaces for the partial slip cases. The predicted fretting fatigue lives are plotted in Fig. 15 as a function of local relative slip amplitude. In addition, the measured lives from Ref. [5] are also plotted in Fig. 15 for comparative purposes. In the gross sliding regime, since wear can lead to the change of element shape greatly and increase the convergence difficulty of contact computation, only the first 100,000 cycles are simulated for the two gross sliding cases. According to the exponential type decay of damage evolution and the damage distribution obtained at 100,000 cycles, it is possible to extrapolate to get the approximate number of cycles to crack initiation. The predicted fretting fatigue lives agree well with the experimental results. The fretting fatigue life decreases when the stroke increases from $32.1 \mu\text{m}$ to $42 \mu\text{m}$ and significant increase in the fretting fatigue life is found when the contact status turns to the gross sliding case. Fig. 16 shows the distribution

Table 5
Predicted results of fretting fatigue life.

Δ (μm)	δ_{local} (μm)	Fatigue life (cycles)	Position of crack initiation	Position of stick–slip interface (p.s.)
32.1	1.357	7.4e4	–0.31	–0.274, 0.347
35	2.047	4.7e4	–0.26	–0.23, 0.39
35.56	2.208	4.4e4	–0.25	–0.22, 0.4
40	3.633	2.5e4	–0.16	–0.14
42	4.408	2.2e4	–0.13	–0.11
43	5.262	27.7e4	–0.63	
44	6.249	49.0e4	–0.71	

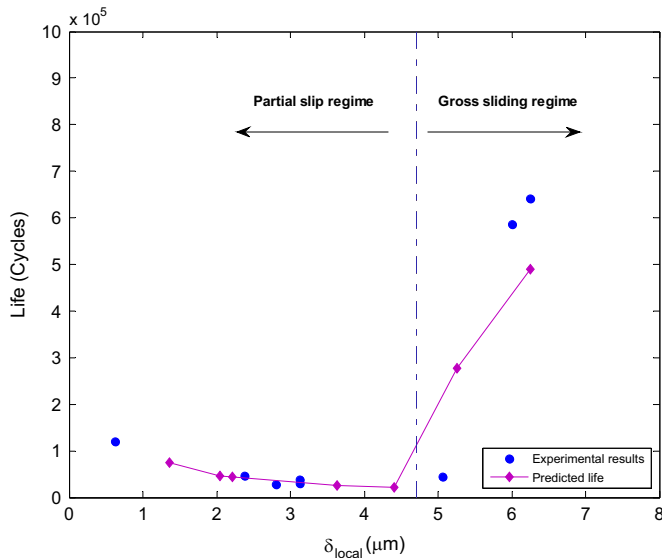


Fig. 15. Predicted fretting fatigue lives along with experimental results.

of damage near the contact zone after 74,000 cycles for $\Delta = 32.1 \mu\text{m}$. The maximum damage is at the left stick–slip interface and very localized. Fig. 17 depicts the distribution of damage near the contact zone after 100,000 cycles for $\Delta = 43 \mu\text{m}$. Damage occurs in a larger region near the left contact edge.

In the partial slip regime, a decrease in fretting fatigue life is predicted as the stroke increases. The same trend is reported in the experiment by Jin and Mall [5] and the investigation by Madge et al. [17]. Until the gross sliding is reached, increase in the stroke results in increasing frictional tangential force Q , as shown in Fig. 18. The contact stresses at the left stick–slip interface increase, thus reducing the predicted fatigue life. The positions of crack initiation for all the partial slip cases are in the slip zone. The stick zone of contact surface moves right as the stroke increases. The right stick–slip interface is near the right contact edge for $\Delta = 40, 42 \mu\text{m}$.

In the gross sliding regime, the increase in the fretting fatigue life is attributed to the reduction of the stress due to wear. The frictional tangential force Q remains unchanged. The predicted fretting fatigue life will also remain unchanged if neglecting the effect of wear as the stroke increases. This trend of fretting fatigue life has been reported by Madge et al. [17]. However, it differs from the results of fretting fatigue tests, which suggests that wear is of key importance to the prediction of fretting fatigue life. As the slip amplitude increases, wear becomes predominant and occurs at the entire contact surface. The contact zone gradually widens with cycling, resulting in the reduction of the stresses, such as contact pressure, shear traction and σ_{xx} . The maximum value of σ_{xx} drops from 976.5 MPa to 677.8 MPa for $\Delta = 43 \mu\text{m}$ as the number of cycles increases, as shown in Fig. 12(b). Therefore, the accumulation of damage slows down significantly.

The two forms of fretting damage, fatigue damage and wear, compete with each other as the stroke increases. In the partial slip regime, fretting fatigue is the main form of failure and fatigue crack can be observed near the contact edge in the fretting fatigue experiment [6]. The predicted fretting fatigue lives for the partial slip cases illustrate this point in this study. In the gross sliding regime, wear slows down the fretting crack nucleation significantly. No cracking is observed within a particular cycles in the fretting wear experiment [46]. Although the fretting fatigue lives are obtained for the gross sliding cases in this investigation, the fatigue lives are much longer than those for the partial slip cases. Wear is more obvious compared to the fatigue crack nucleation in the gross sliding regime.

5.3. The interaction between fatigue damage and wear

The fatigue damage and wear are both considered in this study. Because the damage variable D is not related to the energy wear model and the damage evolution models do not include the variable Δh or h , the relationship between the fatigue damage and wear is indirect. The stress and strain is the bridge to associate the fatigue damage with wear. On the one hand, the fatigue damage is calculated from the stress and strain, meanwhile the fatigue damage results in the redistribution of the stress and strain [11]. On the other hand, the depth of wear scar is related to the shear traction and local relative slip, and the profile of the wear scar affects the stress and strain. Therefore, the fatigue damage and wear interact with each other indirectly through the stress and strain on the contact surface and sub-surface.

5.3.1. Effect of fatigue damage

One group of simulations without consideration of the fatigue damage is carried out to compare with the baseline approach presented in Section 4.3. The elastic–plastic constitutive model and the energy wear model are employed but the effect of fatigue damage is neglected in these simulations. The parameters of the elastic–plastic constitutive model are listed in Table 1. The individual effect of the fatigue damage is investigated through the comparison between the results of the approach neglecting the fatigue damage and the baseline approach.

Fig. 19(a) shows the comparison of contact pressure distribution for $\Delta = 32.1 \mu\text{m}$. The two distributions of contact pressure for the unworn case are identical due to the zero value of the fatigue damage. The peak value of damage increases to 0.48 after 60,000 cycles when the fatigue damage is considered in the baseline approach, as shown in Fig. 10. However, minor variations between the distributions of contact pressure are founded after 60,000 cycles in Fig. 19(a), especially at the location where damage value is small. The effect of damage is insignificant on the evolution of contact stresses including contact pressure and shear traction. The insignificant effect can be attributed to the reason of that damage is localized in two stick–slip interfaces, as shown in Fig. 10. The mechanical properties of a few elements are changed by the fatigue damage. The variation of the whole contact status is not obvious. Minor changes of the shear traction and the local slip are also observed in the computational results, which lead to the insignificant differences of wear scar as shown in Fig. 19(b).

However, the distribution of element stress σ_{xx} is affected by the fatigue damage significantly. Damage weakens the mechanical properties of material directly, and the stress component is calculated at each integration point in the element according to the material mechanical properties. Consequently, the stress σ_{xx} obtained by the approach considering the fatigue damage is smaller than that obtained by the approach neglecting the fatigue damage. Fig. 19(c) shows the comparison of σ_{xx} predicted by the approaches with and without the fatigue damage after 45,000 and 60,000

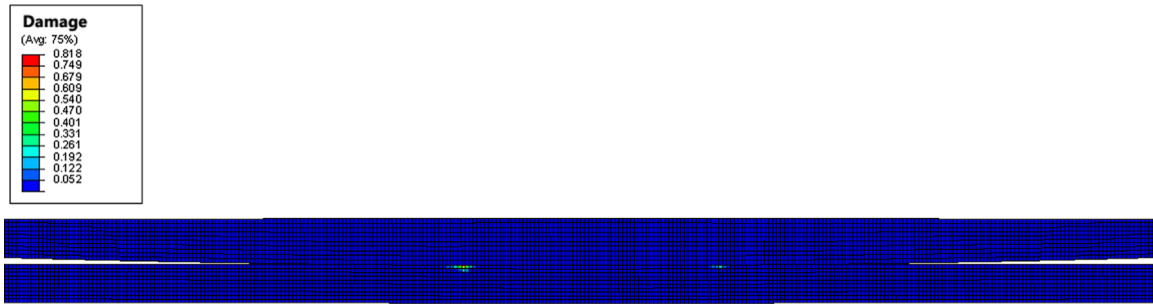


Fig. 16. Distribution of damage near the contact zone after 74,000 cycles for $\Delta = 32.1 \mu\text{m}$.

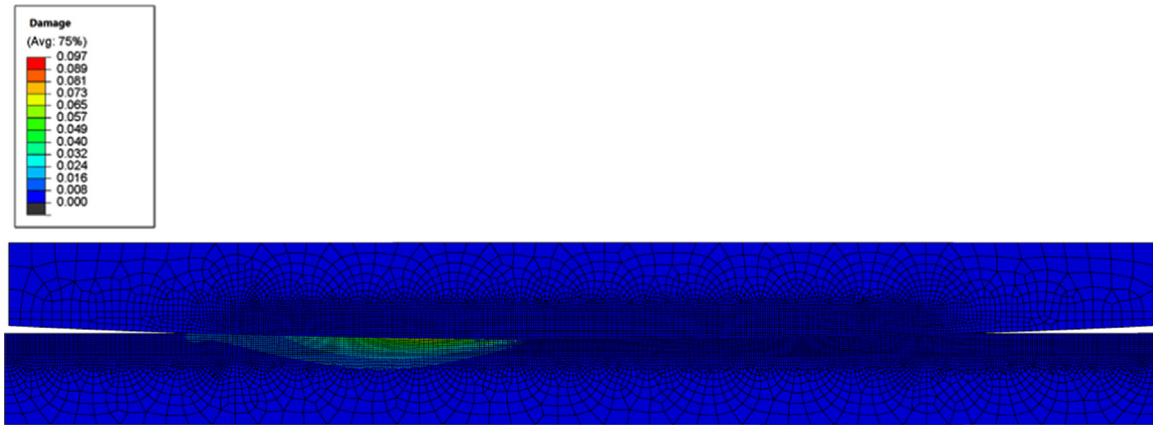


Fig. 17. Distribution of damage near the contact zone after 100,000 cycles for $\Delta = 43 \mu\text{m}$.

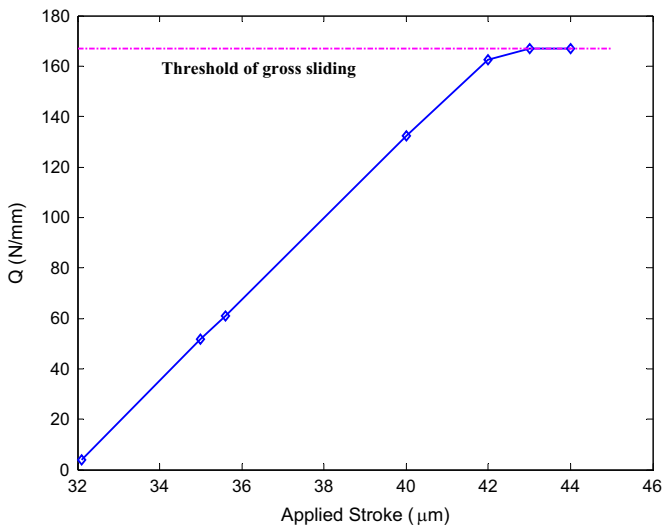


Fig. 18. Frictional tangential force at different strokes.

cycles for $\Delta = 32.1 \mu\text{m}$. The change of the peak value of σ_{xx} obtained by the two approaches can depict the effect of the fatigue damage. The stress σ_{xx} is reduced by the fatigue damage. As the number of loading cycles increases, more severe the fatigue damage grows, more obvious the reduction of the peak value becomes.

5.3.2. Effect of wear

The evolution of contact geometry induced by wear is of key important in this study. The stress, strain and fatigue damage are affected significantly. The results obtained by the approach

considering wear but neglecting the fatigue damage in Section 5.3.1 are used to illustrate the effect of wear.

In the partial slip regime, wear occurs at the slip zone and contact geometry changes, as shown in Fig. 19(b). The contact pressure, shear traction and σ_{xx} increase greatly at the stick-slip interfaces, as well as the strain including equivalent plastic strain. Hence, a conclusion is deduced that wear accelerates the nucleation of fretting fatigue crack.

In the gross sliding regime, wear occurs at the entire contact zone, which is quite different from the case of partial slip. The contact zone widens as the number of loading cycles increases. Fig. 20(a) and (b) shows the evolution of the distribution of contact pressure and σ_{xx} for $\Delta = 43 \mu\text{m}$ by the approach neglecting the fatigue damage. The peak value of σ_{xx} reduces and the location moves to the left evolving contact edge. Therefore, wear delays the nucleation of fretting fatigue crack greatly.

The above analysis about the effect of wear on the fretting fatigue life is carried out according to the evolution of the stress and strain obtained from the wear simulation in Section 5.3.1. Because the effect of wear on the fretting fatigue life in the gross sliding regime has been validated in the literatures [16,17,19], the effect in the partial slip regime is investigated in this study. To validate the deduction about the effect of wear in the partial slip regime, comparative computations neglecting the energy wear model are designed to predict the fretting fatigue life. The damage-coupled elastic-plastic constitutive model and fatigue damage evolution models are employed, of which the parameters are listed in Tables 1–3. The individual effect of wear on the fretting fatigue life is investigated through the comparison between the results of the approach neglecting wear and the baseline approach presented in Section 4.3. The predicted fatigue lives agree with the conclusion about the effect of wear, as illustrated in Fig. 21.

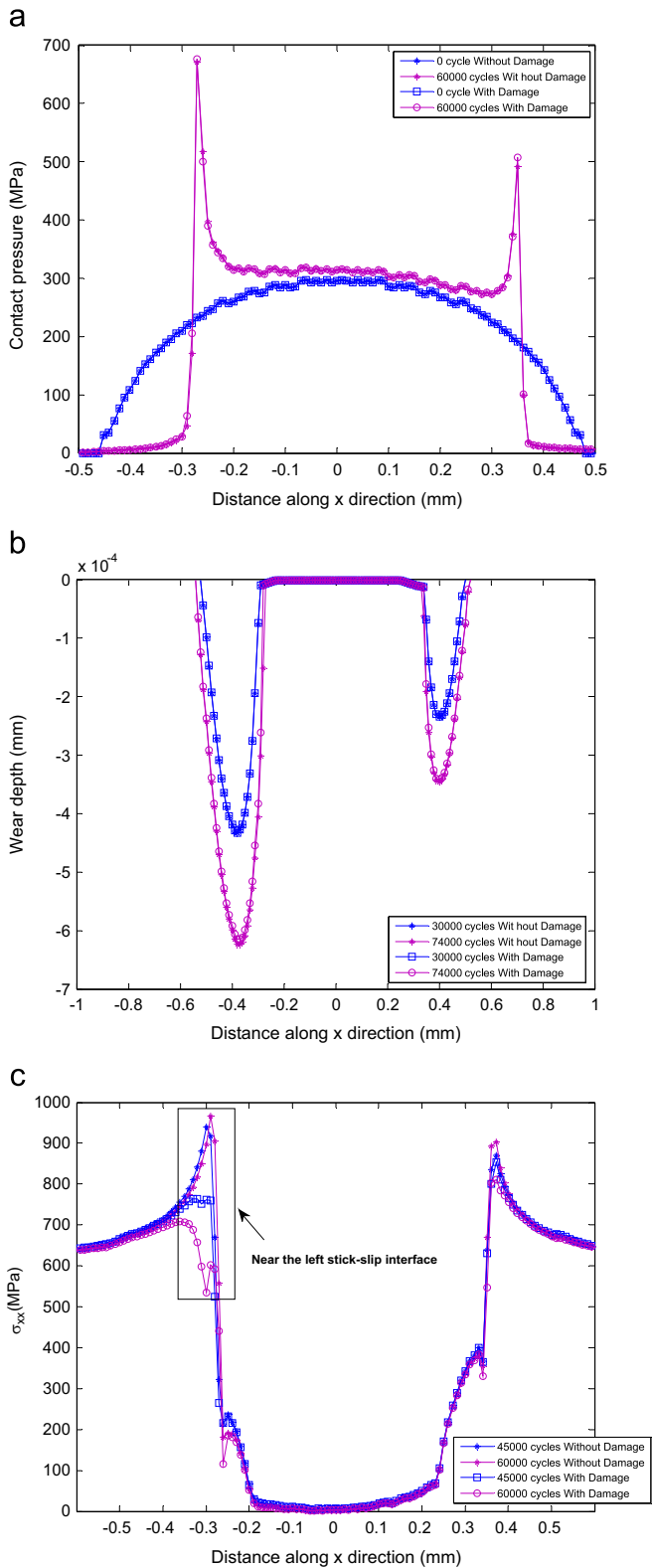


Fig. 19. Comparison of the distribution of (a) contact pressure, (b) wear scar, (c) σ_{xx} by the approaches with and without the fatigue damage for $\Delta = 32.1 \mu\text{m}$.

5.3.3. Combined effects of fatigue damage and wear on σ_{xx}

The evolutions of σ_{xx} shown in Figs. 8(c) and 12(b) are the combined effects of the fatigue damage and wear. As discussed in Sections 5.3.1 and 5.3.2, the effect of wear is opposite with the effect of the fatigue damage in the partial slip regime. Both effects compete with each other as the number of cycles increases. The effect of wear is significant at the beginning of simulation.

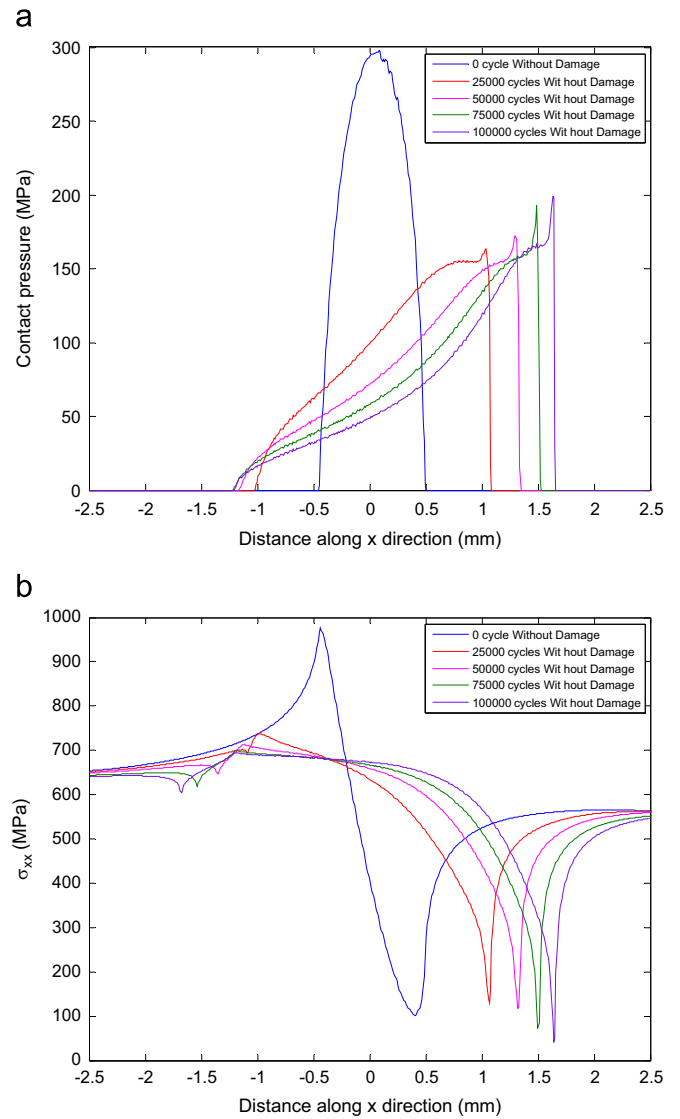


Fig. 20. Evolution of the distribution of (a) contact pressure, (b) σ_{xx} predicted by the approach without the fatigue damage for $\Delta = 43 \mu\text{m}$.

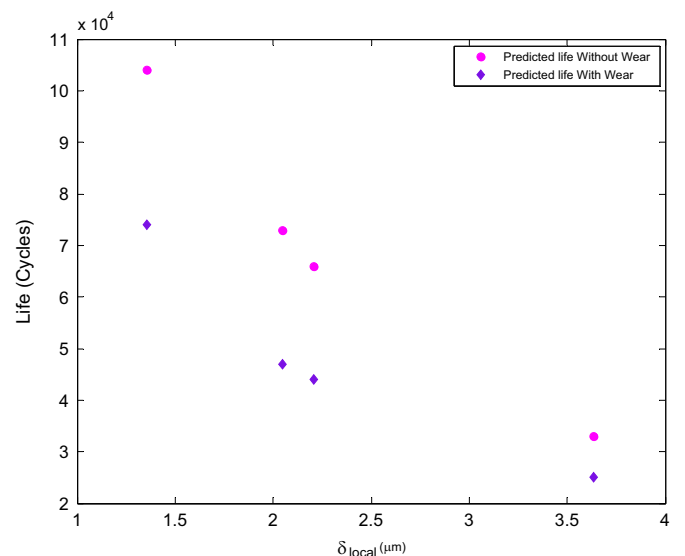


Fig. 21. Comparison of predicted fretting fatigue life by the approaches with and without wear.

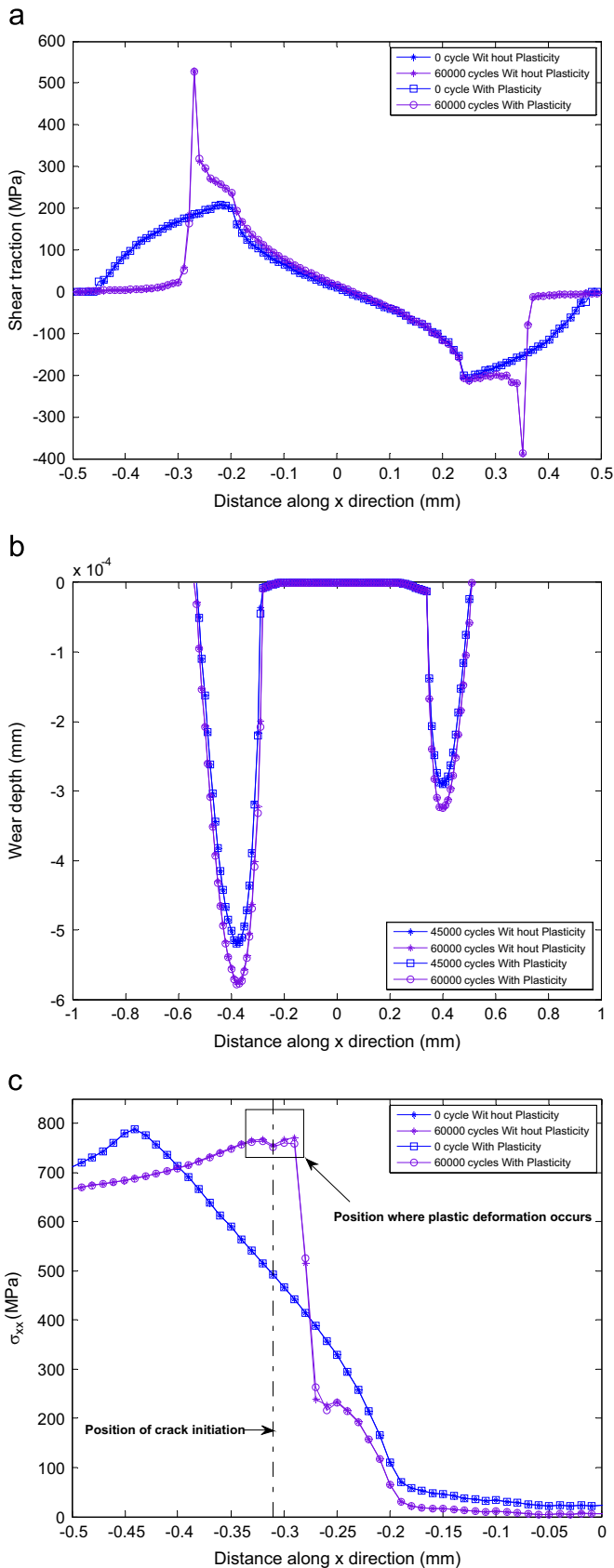


Fig. 22. Comparison of the distribution of (a) shear traction, (b) wear scar, (c) σ_{xx} by the approaches with and without plasticity for $\Delta = 32.1 \mu\text{m}$.

When the fatigue damage becomes more severe, the effect of the fatigue damage is predominant. Therefore, the peak value of σ_{xx} at the left stick–slip interface increases first and then decreases when

the number of cycles increases, as shown in Fig. 8(c). However, the effect of the fatigue damage is consistent with that of wear in the gross sliding regime, both reducing the value of σ_{xx} .

5.4. Effect of plasticity on wear and fretting fatigue

In this study, the maximum equivalent stress is below the initial yield limit for the unworn case. The plastic strain occurs after several cycles at the stick–slip interfaces in the partial slip regime, which indicates the plastic strain is induced by wear and the fatigue damage. Because no plastic deformation occurs within the first 100,000 cycles for the case of gross sliding, the effect of plasticity is investigated in the partial slip regime.

Computations without consideration of plasticity are designed to compare with the baseline approach presented in Section 4.3. The damage-coupled elastic constitutive model, elastic damage model and energy wear model are employed in the computations. Five simulations with different strokes in the partial slip regime are carried out to predict the evolution of wear scar and the fretting fatigue lives.

Plastic deformation occurs firstly at the left stick–slip interface after 24,000 cycles for $\Delta = 32.1 \mu\text{m}$ when considering plasticity in the baseline approach. The peak value of the equivalent plastic strain increases from 4.36×10^{-5} to 1.25×10^{-3} as the number of cycles increases, as shown in Fig. 9. Fig. 22(a), (b) and (c) shows the comparison of the distribution of shear traction, wear scar and σ_{xx} for $\Delta = 32.1 \mu\text{m}$, respectively. The effect of plasticity on the shear traction and wear scar is not evident. The small and localized plastic deformation can be the main reason for the insignificant effect of plasticity. The value of σ_{xx} obtained by the approach neglecting plasticity is slightly larger than that by the baseline approach near the location of crack initiation after 60,000 cycles.

The comparison of the fretting fatigue lives are shown in Fig. 23. The fatigue lives predicted by the approach neglecting plasticity are shorter than that obtained by the baseline approach. Two aspects of the reason can be deduced: (1) The stress is over-predicted by the elastic constitutive model. In fact, the mechanical behavior of material can be modeled more accurately by considering plasticity when plastic deformation occurs. (2) Because the plastic damage related to the plastic strain is small, the fretting fatigue life is governed by the dominant elastic

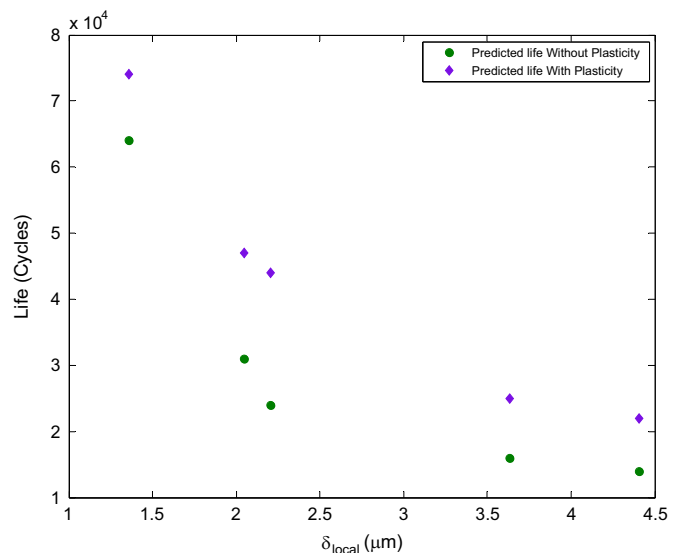


Fig. 23. Comparison of predicted fretting fatigue life by the approaches with and without plasticity.

damage. Therefore, the larger stress obtained by the approach neglecting plasticity results in the shorter fretting fatigue life. Although the plastic damage is small when considering plasticity in the fretting fatigue, the reasonable calculation of the stress is critical for the fretting fatigue life prediction. The comparison between the results also illustrates the necessity of considering plasticity in the damage mechanics approach.

6. Conclusions

A damage mechanics approach to fretting fatigue is presented with consideration of cyclic plasticity and wear. Damage-coupled elastic–plastic constitutive model is employed in this study. The energy wear model is adopted to take the effect of wear on contact geometry and mechanics variables into account. A finite element implementation is developed and fretting fatigue lives are predicted by the damage mechanics approach for partial slip cases and gross sliding cases. The approach presented in this study has several features as follows:

- Fatigue damage and wear are both considered in the damage mechanics approach. The interaction of fatigue damage and wear is analyzed in this study.
- Damage-coupled elastic–plastic constitutive model including nonlinear kinematic hardening is employed to calculate the stress and strain when material is damaged. Damage is divided into two parts, elastic damage and plastic damage, which are related to the cyclic stress and accumulated plastic strain, respectively.
- Plastic deformation is attributed to the evolution of the fatigue damage and the change of contact geometry induced by wear. The effect of cyclic plasticity on wear and fretting fatigue is investigated.
- The damage-coupled elastic–plastic constitutive model, damage evolution models and energy wear model are implemented in the numerical algorithm. The progressive damage is simulated in the finite element implementation, as well as the evolution of wear scar.

Some key findings are

- In terms of partial slip case, the contact pressure, shear traction and σ_{xx} increase greatly at the stick–slip interfaces due to the variation of contact geometry induced by wear. Insignificant effect of damage on the contact pressure and shear traction is founded but damage reduces the value of σ_{xx} significantly. An obvious competition between the effects of fatigue damage and wear on σ_{xx} is investigated in this study. Plastic deformation occurs at stick–slip interfaces after a number of cycles due to wear and the fatigue damage. Wear accelerates the nucleation of fretting fatigue crack in the partial slip regime.
- In terms of gross sliding case, the stresses decreases due to the widened contact zone induced by wear. No plastic strain is founded within the particular cycles. Wear delays the nucleation of fretting fatigue crack greatly.
- No evident effect of plasticity on the wear scar is observed in the partial slip case. However, the effect of plasticity on the fretting fatigue life illustrates the necessity of considering plasticity in the damage mechanics approach.

Acknowledgment

Financial support by the National Natural Science Foundation of China (11002010) is gratefully acknowledged.

References

- [1] Hills DA, Nowell D. Mechanics of fretting fatigue. Boston: Kluwer Academic Publishers; 1994.
- [2] Zhang T, Harrison NM, McDonnell PF, McHugh PE, Leen SB. A finite element methodology for wear–fatigue analysis for modular hip implants. *Tribol Int* 2013;65:113–27.
- [3] Mohd Tobi AL, Ding J, Bandak G, Leen SB, Shipway PH. A study on the interaction between fretting wear and cyclic plasticity for Ti–6Al–4V. *Wear* 2009;267:270–82.
- [4] Jin O, Mall S. Influence of contact configuration on fretting fatigue behavior of Ti–6Al–4V under independent pad displacement condition. *Int J Fatigue* 2002;24:1243–53.
- [5] Jin O, Mall S. Effects of slip on fretting behavior: experiments and analysis. *Wear* 2004;256:671–84.
- [6] Jin O, Mall S. Effects of independent pad displacement on fretting fatigue behavior of Ti–6Al–4V. *Wear* 2002;253:585–96.
- [7] Nakazawa Kozo, Maruyama Noria, Hanawa Takao. Effect of contact pressure on fretting fatigue of austenitic stainless steel. *Tribol Int* 2003;36:79–85.
- [8] Ramakrishna NK, Ganesh Sundara Raman S. Effect of contact pressure on fretting fatigue behavior of Al–Mg–Si alloy AA6061. *Int J Fatigue* 2005;27:283–91.
- [9] Szolwinski Matthew P, Farris Thomas N. Mechanics of fretting crack formation. *Wear* 1996;198:93–107.
- [10] Lykins Christopher D, Mall Shankar, Jain Vinod. An evaluation of parameters for predicting fretting fatigue crack initiation. *Int J Fatigue* 2000;22:703–16.
- [11] Zhang T, McHugh PE, Leen SB. Finite element implementation of multiaxial continuum damage mechanics for plain and fretting fatigue. *Int J Fatigue* 2012;44:260–72.
- [12] Hojjati-Talemi Reza, Wahab Magd Abdel. Fretting fatigue crack initiation lifetime predictor: using damage mechanics approach. *Tribol Int* 2013;60:176–86.
- [13] Walvekar Aditya A, Leonard Benjamin D, Sadeghi Farshid, Jalalhamadi Behrooz, Bolander Nathan. An experimental study and fatigue damage model for fretting fatigue. *Tribol Int* 2014;79:183–96.
- [14] Aghdam AB, Beheshti Ali, Khonsari MM. Prediction of crack nucleation in rough line-contact fretting via continuum damage mechanics approach. *Tribol Lett* 2014;53:631–43.
- [15] McColl IR, Ding J, Leen SB. Finite element simulation and experimental validation of fretting wear. *Wear* 2004;256:1114–27.
- [16] Madge JJ, Leen SB, Shipway PH. The critical role of fretting wear in the analysis of fretting fatigue. *Wear* 2007;263:542–51.
- [17] Madge JJ, Leen SB, McColl IR, Shipway PH. Contact-evolution based prediction of fretting fatigue life: effect of slip amplitude. *Wear* 2007;262:1159–70.
- [18] Leonard Benjamin D, Patil Pankaj, Slack Trevor S, Sadeghi Farshid, Shinde Sachin, Mittelbach Marc. Fretting wear modeling of coated and uncoated surfaces using the combined finite-discrete element method. *J Tribol* 2011;133:021601.
- [19] Zhang T, McHugh PE, Leen SB. Computational study on the effect of contact geometry on fretting behavior. *Wear* 2011;271:1462–80.
- [20] Fouvry S, Liskiewicz T, Kapsa PH, Hannel S, Sauger E. An energy description of wear mechanisms and its applications to oscillating sliding contacts. *Wear* 2003;255:287–98.
- [21] Ghosh Arnab, Leonard Ben, Sadeghi Farshid. A stress based damage mechanics model to simulate fretting wear of Hertzian line contact in partial slip. *Tribol Int* 2013;307:87–99.
- [22] Lemaitre J, Chaboche JL. Mechanics of solid materials. Cambridge: Cambridge University Press; 1994.
- [23] Yu SW, Feng XQ. Damage mechanics. Beijing: Tsinghua University Press; 1997.
- [24] Lemaitre J, Rodrigue D. Engineering damage mechanics. Berlin: Springer; 2005.
- [25] Armstrong PJ, Frederick CO. A mathematical representation of the multiaxial Bauschinger effect. CEBG Report, RD/B/N731, Berkely, UK: Berkeley Nuclear Laboratories; 1966.
- [26] Chaboche JL. A review of some plasticity and viscoplasticity constitutive theories. *Int J Plast* 2008;24:1642–93.
- [27] Abdel-Karim Mohammad. Modified kinematic hardening rules for simulations of ratchetting. *Int J Plast* 2009;25:1560–87.
- [28] Abdel-Karim Mohammad. An evaluation for several kinematic hardening rules on prediction of multiaxial stress-controlled ratchetting. *Int J Plast* 2010;26:711–30.
- [29] Naderi M, Hoseini SH, Khonsari MM. Probabilistic simulation of fatigue damage and life scatter of metallic components. *Int J Plast* 2013;43:101–15.
- [30] Chaboche JL, Lesne PM. A non-linear continuous fatigue damage model. *Fatigue Fract Eng Mater Struct* 1988;11:1–17.
- [31] Marmi AK, Habraken AM, Duchene L. Multiaxial fatigue damage modeling at macro scale of Ti–6Al–4V alloy. *Int J Fatigue* 2009;31:2031–40.
- [32] Sines G. Behavior of metals under complex static and alternating stresses. Metal fatigue. New York: McGraw Hill; 1959: 145–69.
- [33] Kang GZ, Liu YJ, Ding J, Gao Q. Uniaxial ratcheting and fatigue failure of tempered 42CrMo steel: damage evolution and damage-coupled visco-plastic constitutive model. *Int J Plast* 2009;25:838–60.
- [34] Warhadpande Anurag, Sadeghi Farshid, Kotzalas Michael N, Doll Gary. Effects of plasticity on subsurface initiated spalling in rolling contact fatigue. *Int J Fatigue* 2012;36:80–95.

- [35] Fridrici V, Fouvry S, Kapsa PH. Effect of shot peening on the fretting wear of Ti–6Al–4V. *Wear* 2001;250:642–9.
- [36] Magaziner RS, Jain VK, Mall S. Wear characterization of Ti–6Al–4V under fretting-reciprocating sliding conditions. *Wear* 2008;264:1002–14.
- [37] Military Handbook – MIL-HDBK-5H: Metallic materials and elements for aerospace vehicle structures (Knovel interactive ed.). US Department of Defense; 1998. <http://dx.doi.org/10.1016/j.ijfatigue.2012.04.011>.
- [38] Wu XR. Handbook of mechanics properties of aircraft structure metals. Beijing: Aviation Industry Press; 1997.
- [39] Sabelkin V, Mall S. Investigation into relative slip during fretting fatigue under partial slip contact condition. *Fatigue Fract Eng Mater Struct* 2005;28:809–24.
- [40] Johnson KL. Contact mechanics. Cambridge: Cambridge University Press; 1985.
- [41] Simo JC, Taylor RL. Consistent tangent operator for rate-independent elasto-plasticity. *Comput Methods Appl Mech Eng* 1985;48:101–18.
- [42] Kang. GZ. A visco-plastic constitutive model for ratcheting of cyclically stable materials and its finite element implementation. *Mech Mater* 2004;36:299–312.
- [43] Kang. GZ. Ratchetting: recent progresses in phenomenon observation, constitutive modeling and application. *Int J Fatigue* 2008;30:1448–72.
- [44] Belytschko Ted, Liu Wing Kam, Moran Brian. Nonlinear finite elements for continua and structures. Chichester: Wiley; 2000.
- [45] ABAQUS/Standard version 6.10. User manual. Rhode Island, USA: Hibbit Karlsson and Sorensen Inc.; 2010.
- [46] Ding J, Bandak G, Leen SB, Williams EJ, Shipway PH. Experimental characterization and numerical simulation of contact evolution effect on fretting crack nucleation for Ti–6Al–4V. *Tribol Int* 2009;42:1651–62.